Gap-soliton propagation in nonuniform gratings

Neil G. R. Broderick and C. Martijn de Sterke
School of Physics and Optical Fibre Technology Centre, University of Sydney, Sydney, New South Wales 2006, Australia
(Received 27 October 1994)

The effects of nonuniform gratings on gap-soliton propagation are treated theoretically using an effective particle approach. The method is accurate and quick over a wide range of parameters. It also provides accurate predictions about the stability of stationary gap solitons at an interface.

PACS number(s): 42.81.Dp, 42.50.Rh

I. INTRODUCTION

Theoretical studies of finite nonlinear Bragg gratings [1,2] have shown that they can exhibit bistable optical behavior. At low intensities the grating is highly reflective, but when the intensity is sufficient the transmission can approach unity. It has been shown that when the grating is highly reflective the electric field inside it decays nearly exponentially; in contrast, the electric field profile associated with the highly *transmissive* states peaks distinctively inside the grating as found by Winful *et al.* [1]. These peaked field profiles have been associated with stationary gap solitons [3]. Later Aceves and Wabnitz [4] showed that gap solitons can traverse the grating at any speed between zero and the speed of light. In addition, they derived analytic expressions for gap solitons in an infinite uniform grating by noting the similarities between the nonlinear coupled mode equations (NLCMEs) (used to describe Bragg gratings) and the exactly integrable massive Thirring model. Gap solitons were found to have frequencies that lie within the band gap of a uniform grating; they are thus manifestly nonlinear as in the linear limit no pulse solutions exist within this frequency range.

Recent experiments [5] have demonstrated all-optical switching in optical waveguides. These experiments were performed in a SiO_2 waveguide with the nonlinearity being caused by free carriers. Although free carriers provide a strong nonlinearity, they have a response time of about 1 ns and so only the continuous wave properties of the grating were examined. In contrast, gap-soliton propagation requires nonlinearities with a subpicosecond response time, which typically are much weaker [6]. Thus the intensities required to see nonlinear propagation effects in gratings are much larger.

We have recently [7,8] proposed a scheme for launching gap solitons in nonuniform gratings, which significantly reduces the power needed. In particular we examined the properties of step gratings as these are the simplest example of nonuniform gratings. This method involves coupling light into linear resonances of the grating, which then forms a gap soliton. By exciting a resonance of the grating, a major reduction in the required launch power compared to the uniform case is possible. However, the propagation of the gap solitons in these nonuniform gratings is considerably more complicated than for the case of a uniform grating. This paper continues our previous work by examining the propagation of gap solitons in nonuniform gratings; in particular we consider the effect of an abrupt interface on gap solitons.

The presence of an interface allows the existence of additional stationary solutions to the coupled mode equations. These solutions have a discontinuity in the derivates of the field amplitudes at the interface, in contrast to the ordinary gap solitons. At the interface a traveling gap soliton can be reflected, transmitted, or in extreme cases broken up into multiple reflected solitons. Aceves, Newell, and Moloney [9] have successfully treated the similar problem for the nonlinear Schrödinger equation (NLSE) using an effective particle picture (EPP). As the NLCME reduce to the NLSEs in the appropriate limit, an EPP approach would be expected to be valid, at least for some parameter range.

Since the NLCMEs reduce to the massive Thirring model (MTM) in the stationary limit, the stationary gap solitons present at an interface are solutions to the MTM as well. Our EPP approach applies to the MTM and by way of comparison we present the results for both the MTM and the NLCME. As the MTM is exactly integrable, we expect that an EPP approach would work better and we find that this is indeed the case.

II. THE EFFECTIVE PARTICLE APPROACH

Starting from Maxwell's equations with a periodic refractive index and a nonlinear polarization one can derive the nonlinear coupled mode equations governing the evolution of the slowly varying envelopes $\mathcal{F}_+$ and $\mathcal{F}_-$ of the forward and backward propagating electric fields, respectively [10]. In the presence of perturbations these equations have to be modified. Using a complex matrix V_{ij} to describe the perturbations, the modified coupled mode equations can be written as

$$i\frac{\partial \mathcal{F}_+}{\partial x}+\frac{i}{v_g}\frac{\partial \mathcal{F}_+}{\partial t}+\kappa\mathcal{F}_-+2\Gamma_x|\mathcal{F}_-|^2\mathcal{F}_+ +\Gamma_s|\mathcal{F}_+|^2\mathcal{F}_+ + V_{11}(x)\mathcal{F}_+ + V_{12}(x)\mathcal{F}_- = 0, \quad (1)$$

$$-i\frac{\partial \mathcal{F}_-}{\partial x} + \frac{i}{v_g}\frac{\partial \mathcal{F}_-}{\partial t} + \kappa \mathcal{F}_+ + 2\Gamma_x|\mathcal{F}_+|^2\mathcal{F}_-$$

$$+\Gamma_s|\mathcal{F}_-|^2\mathcal{F}_- + V_{21}(x)\mathcal{F}_+ + V_{22}(x)\mathcal{F}_- = 0. \quad (2)$$

The massive Thirring model equations are obtained by setting $\Gamma_s = 0$ and $V_{ij} = 0$. The group velocity v_g, which determines the speed of the fields in the absence of a grating, is set equal to unity by a rescaling of the time parameter t. The parameter κ describes the grating strength. The terms Γ_s and Γ_x determine the strength of the self- and the cross-phase modulation, respectively. In an optical Bragg grating κ, Γ_s, and Γ_x are given by [11]

$$\kappa = \frac{\pi \Delta n}{\lambda}, \quad \Gamma_x = \Gamma_s = \frac{4\pi \bar{n}}{\lambda Z} n^{(2)}, \quad (3)$$

where $\bar{n}$ is the average refractive index, Δn is the maximum refractive index change of the grating, $n^{(2)}$ is the nonlinear refractive index, Z is the vacuum impedance, and λ is the free space wavelength of the light.

The perturbations to the fields in Eqs. (1) and (2) are given by the complex matrix V_{ij}. As we have assumed that the perturbations are proportional to the fields, the matrix V is unable to represent the effects of a driving term; however, most other perturbations can be represented in this manner. If V is Hermitian, then the medium is lossless, which is the case under consideration.

In the absence of any perturbations ($V_{ij} = 0$) the MTM ($\Gamma_s = 0$) possesses the following one-soliton solution centered at $x = x_0$, where ζ has been used to distinguish it from the NLCME soliton [12]:

$$\zeta_+(x,t) = \sqrt{\frac{\kappa}{2\Gamma_x}}\frac{1}{\Delta} e^{i\sigma} \sin(\delta)\,\mathrm{sech}(\theta - i\delta/2), \quad (4)$$

$$\zeta_-(x,t) = -\sqrt{\frac{\kappa}{2\Gamma_x}}\Delta\, e^{i\sigma} \sin(\delta)\,\mathrm{sech}(\theta + i\delta/2), \quad (5)$$

where

$$\theta = \gamma\kappa \sin\delta(x - x_0 - \chi t), \quad (6)$$

$$\sigma = \gamma\kappa \cos\delta(\chi x - t - t_0), \quad (7)$$

$$\gamma = \frac{1}{\sqrt{1-\chi^2}}, \quad \Delta = \left(\frac{1-\chi}{1+\chi}\right)^{1/4}. \quad (8)$$

In terms of this solution we can write the solitary wave solutions to the NLCME as [4]

$$\mathcal{F}_\pm(x,t) = \alpha\zeta_\pm(x,t)e^{i\eta(\theta)}, \quad (9)$$

where

$$\alpha = \left(1 + \frac{\Gamma_s}{2\Gamma_x}\frac{1+\chi^2}{1-\chi^2}\right)^{-\frac{1}{2}} \quad (10)$$

and $\eta(\theta)$ is a phase factor, the form of which is not important here. These solutions for both the MTM and the NLCME are characterized by three parameters δ, χ, and t_0. The parameter t_0 defines a constant phase and in the absence of any other fields it is unimportant. The velocity of the gap soliton is given by χv_g and hence χ must lie in the range $-1 < \chi < 1$. The third parameter δ determines the width, height, and central frequency of the gap soliton and lies in the range $0 < \delta < \pi$. In the case where both δ and χ are small, the solitary wave solution reduces to the NLSE soliton [11]. When $\chi = 0$ or $\Gamma_s = 0$ the phase factor η in Eq. (9) is identically zero and the solution reduces to the MTM soliton.

In the presence of perturbations analytic soliton solutions do not usually exist. However, if the perturbations are small, then we can make the EPP assumption that we can always describe the field as a gap soliton. Thus, in the EPP approach we are interested in the time evolution of δ and χ as these uniquely define the gap-soliton up to a constant phase factor. The aim of this section is to derive equations of motion for δ and χ. This is done by considering a small set of global moments of the field that in the absence of any perturbations, completely characterize the gap soliton. The moments chosen are analogous to the moments used by Aceves *et al.* [9]. The moments we use are given below, where they are defined ($\equiv$) and then evaluated for the particular case of a gap soliton ($=$): the energy Q

$$Q \equiv \int_{-\infty}^{+\infty} \left(|\mathcal{F}_+|^2 + |\mathcal{F}_-|^2\right) dx = \frac{2\delta\alpha^2}{\Gamma_x}, \quad (11)$$

the average position $\bar{x}$

$$\bar{x} \equiv \frac{1}{Q}\int_{-\infty}^{+\infty} x\left(|\mathcal{F}_+|^2 + |\mathcal{F}_-|^2\right) dx = x_0 + \chi t, \quad (12)$$

the velocity v

$$v \equiv \frac{1}{Q}\int_{-\infty}^{+\infty} \left(|\mathcal{F}_+|^2 - |\mathcal{F}_-|^2\right) dx = \chi, \quad (13)$$

and the momentum $\mathcal{P}$

$$\mathcal{P} \equiv -i\int_{-\infty}^{+\infty} \left(\mathcal{F}_+^*\partial_x\mathcal{F}_+ + \mathcal{F}_-^*\partial_x\mathcal{F}_-\right) dx \quad (14)$$

$$= \frac{2\kappa\chi\gamma}{\Gamma_x}\alpha^2 \sin\delta + \frac{4\kappa\Gamma_s\chi\gamma^3}{\Gamma_x^2}\alpha^4(\sin\delta - \delta\cos\delta).$$

In Eqs. (11)–(14) the results for the MTM soliton can be obtained by setting $\alpha = 1$ and $\Gamma_s = 0$. Note that both the energy Q and the momentum $\mathcal{P}$ are conserved quantities of the unperturbed equations [12,13]. The equations also possess a third conserved quantity, namely, the Hamiltonian [12], that is not used in this approach. These moments are chosen so that if a gap-soliton is present, then knowledge of these moments allows us to reconstruct the gap soliton up to a constant phase factor.

Using the coupled mode equations [Eqs. (1) and (2)] the time derivates of the above moments [Eqs. (11)–(14)] can easily be calculated; taking the perturbation matrix V to be Hermitian, we find

$$\frac{dQ}{dt} = 0, \quad (15)$$

$$\frac{d\bar{x}}{dt} = v, \quad (16)$$

$$\frac{dv}{dt} = \frac{4\kappa}{Q}\int_{-\infty}^{+\infty} \mathrm{Im}(\mathcal{F}_+\mathcal{F}_-^*)dx, \tag{17}$$

$$\frac{d\mathcal{P}}{dt} = \int_{-\infty}^{+\infty}\left[|\mathcal{F}_+|^2\frac{\partial V_{11}}{\partial x} + |\mathcal{F}_-|^2\frac{\partial V_{22}}{\partial x} + 2\mathrm{Re}\left(\mathcal{F}_+\,\mathcal{F}_-^*\frac{\partial V_{21}}{\partial x}\right)\right]dx. \tag{18}$$

Equation (15) expresses energy conservation, as discussed in Sec. I. Equation (16) confirms that the definitions of position and the velocity given by Eqs. (12) and (13) are mutually consistent.

Though Eqs. (15)–(18) are exact, the integrals are in general difficult to evaluate since it is necessary to know the fields exactly at all times (i.e., we have to solve the coupled mode equations). To get a simpler set of equation we use the EPP assumption, i.e., the field is always described by a gap-soliton. In particular this implies that $v = \chi$. We now have four equations for the three unknowns δ, χ, and the center of the gap soliton $\bar{x}$, so one equation is redundant. Following Aceves *et al.* [9] we work with $\mathcal{P}$ and drop Eq. (17). Since $\mathcal{P}$, unlike v, is a conserved quantity of the unperturbed equations, $\mathcal{P}$ is more sensitive to the effects of the perturbations. This is reflected in the perturbations V_{ij} appearing explicitly in Eq. (18), but not in Eq. (17). Of the three remaining equations, Eq. (15) in conjunction with Eq. (11) allows $\delta(t)$ to be expressed in terms of the initial energy and $\chi(t)$, thus eliminating δ from the system of equations. We now have two equations [Eqs. (16) and (18)] for the two remaining unknowns $\bar{x}$ and χ. Assuming that the integrals in Eq. (18) can be done exactly using the expressions for the gap soliton we have reduced the two partial differential equations [Eqs. (1) and (2)] to two ordinary differential equations [Eqs. (16) and (18)].

For perturbations, involving gain or loss Eqs. (15)–(18) slightly change; in particular $dQ/dt \neq 0$ as expected. Also Eq. (16) contains extra terms that indicate that for nonuniform gain, the center of mass of the soliton eventually lies in the region of highest gain. We note further that earlier work on the effects of gain and loss [14,15] on gap solitons can be reproduced using the appropiate non-Hermitian V_{ij}.

Having derived the EPP equations [Eqs. (16) and (18)], we next present two applications. The first deals with the stability of stationary solutions at interfaces and the second with the motion of gap solitons at interfaces.

III. STABILITY OF STATIONARY SOLITON SOLUTIONS

The EPP can be used to predict the stability of nonlinear surface waves. In this section we first derive the exact expressions for the surface waves and then show how in one particular case the EPP provides insight into the stability of these waves. Although we only present one case in detail, the EPP can be used for determining the stability for more general perturbations.

A. Stationary solutions at an interface

While the soliton solutions [Eq. (9)] are valid for uniform gratings, we are interested in gratings that are nonuniform. In particular we consider a grating consisting of two half infinite uniform gratings joined at the origin ($x = 0$), with the grating parameters changing discontinuously there [9]. The parameters for $x < 0$ are denoted by the subscript l, e.g., κ_l, while the subscript r denotes the right-hand grating ($x > 0$). We also assume that the right-hand grating can have an arbitrary phase ϕ with respect to the left-hand grating.

We obtain stationary soliton solutions by assuming that we have part of a gap soliton in each half, but peaked at different positions and by matching the fields at $x = 0$. In particular, for $x < 0$ we have

$$\mathcal{F}_{l,+}(x,t) = \alpha\sqrt{\frac{\kappa_l}{2\Gamma_{xl}}}\,e^{-i\kappa_l\cos\delta_l t}\,\sin(\delta_l) \times \mathrm{sech}\left[\kappa_l\sin\delta_l(x-x_l) - i\delta_l/2\right]. \tag{19}$$

For $x > 0$ we have a similar solution, only peaked at $x = x_r$. There is now a phase factor $-\phi/2$ due to the phase difference ϕ between the two gratings and also an overall phase factor ψ and thus

$$\mathcal{F}_{r,+}(x,t) = e^{i\psi}e^{-i\phi/2}\alpha\sqrt{\frac{\kappa_r}{2\Gamma_{xr}}}\,e^{-i\kappa_r\cos\delta_r t}\,\sin(\delta_r) \times \mathrm{sech}\left[\kappa_r\sin\delta_r(x-x_r) - i\delta_r/2\right]. \tag{20}$$

The solutions for $\mathcal{F}_-$ are

$$\mathcal{F}_{l,-}(x,t) = -[\mathcal{F}_{l,+}(x,t)]^* e^{-2i\kappa_l\cos\delta_l t},$$
$$\mathcal{F}_{r,-}(x,t) = -e^{2i\psi}[\mathcal{F}_{r,+}(x,t)]^* e^{-2i\kappa_r\cos\delta_r t}. \tag{21}$$

To obtain a solution for $-\infty < x < \infty$ we need to match the solutions for $\mathcal{F}_+$ and $\mathcal{F}_-$ at $x = 0$. Assuming that we

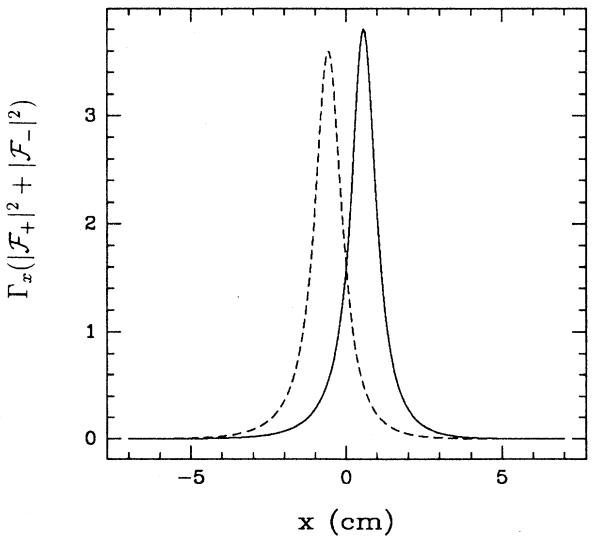

FIG. 1. Plot of field intensities for stationary gap solitons with $\delta_l = 2.5$. The solid line shows the stationary solution peaked in the high κ grating, while the dotted line shows the solution peaked in the low κ medium. The interface is at $x = 0$ with $\kappa_l = 1\ \mathrm{cm}^{-1}$ and $\kappa_r = 1.1\ \mathrm{cm}^{-1}$.

know $\mathcal{F}_+$, then Eq. (21) implies that $\exp(2i\psi) = 1$ or that $\psi = 0$ or $\psi = \pi$. Equating the real and imaginary parts of $\mathcal{F}_{l,+}(0,t)$ and $\mathcal{F}_{r,+}(0,t)$, this leads to two equations for $\delta_l, \delta_r, x_l, x_r$. The exponential time dependence of each equation implies that

$$\kappa_l \cos\delta_l = \kappa_r \cos\delta_r. \tag{22}$$

Factoring out the time dependence we find two equations for x_l and x_r,

$$\begin{pmatrix} c_r \\ s_r \end{pmatrix} = \pm \frac{\sin\delta_r}{\sin\delta_l}\sqrt{\frac{\Gamma}{\kappa}} \begin{pmatrix} \frac{\cos(\delta_l/2)\cos(\phi/2)}{\cos(\delta_r/2)} & \frac{-\sin(\delta_l/2)\sin(\phi/2)}{\cos(\delta_r/2)} \\ \frac{\cos(\delta_l/2)\sin(\phi/2)}{\sin(\delta_r/2)} & \frac{-\sin(\delta_l/2)\cos(\phi/2)}{\sin(\delta_r/2)} \end{pmatrix} \begin{pmatrix} c_l \\ s_l \end{pmatrix} \tag{23}$$

where

$$c_l = \cosh(\kappa_l \sin\delta_l x_l), \quad s_l = \sinh(\kappa_l \sin\delta_l x_l), \tag{24}$$

$$c_r = \cosh(\kappa_r \sin\delta_r x_r), \quad s_r = \sinh(\kappa_r \sin\delta_r x_r), \tag{25}$$

$$\kappa = \frac{\kappa_l}{\kappa_r}, \quad \Gamma = \frac{\Gamma_l}{\Gamma_r}. \tag{26}$$

The top sign in Eq. (23) corresponds to the case where $\psi = 0$, while the bottom sign implies $\psi = \pi$. Using $c_r^2 - s_r^2 = 1$ we can eliminate x_r, which leaves us with one equation for x_l. Similarly we can eliminate x_l to get an equation for x_r.

If the phase difference ϕ between the two gratings is either 0 or π, Eqs. (23) can be solved exactly for x_l and x_r. In both these cases, in order for solutions to exist, it is necessary for $\delta_l > \pi/2$. Recall that the energy of a gap soliton is proportional to δ, so a minimum value for δ implies a minimum energy for the solution to exist. We then find two stationary solutions for if x_l and x_r are solutions to Eq. (23), then so are $-x_l$ and $-x_r$. It is found that the signs of x_l and x_r are the same, hence the solution is single peaked. A typical solution is shown in Fig. 1.

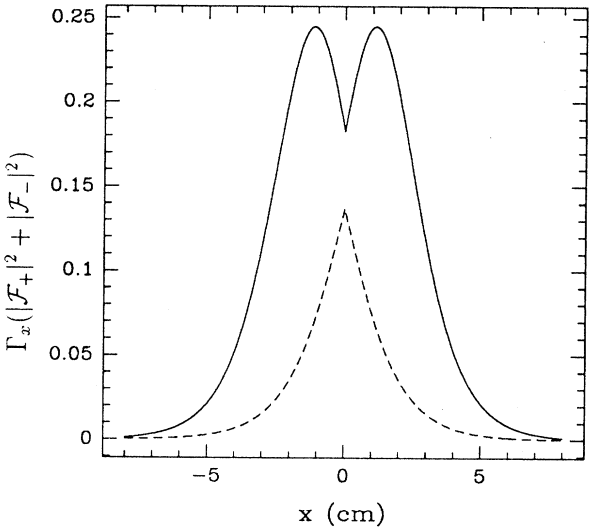

FIG. 2. Plots of typical stationary solutions when a phase change is introduced between the two gratings. The solid line shows the field intensity for a soliton with $\delta = 0.5$ with a grating phase change of $\phi = 0.5$. The dotted line gives the intensity for a soliton with $\delta = 0.45$ and for a phase change of $\phi = -0.5$. The grating has a strength $\kappa = 1$ cm^{-1}.

If we allow an arbitrary phase difference ψ between the two gratings, then Eqs. (23) have to be solved numerically. Here we find that no restriction can be placed on δ_l in contrast to the previous case. Also here we find that x_l and x_r can have different signs leading to either a two peaked solution if $x_l < 0$ and $x_r > 1$ or a "zero" peaked solution if $x_l > 0$ and $x_r < 0$. Such solutions are shown in Fig. 2.

We note in passing that ultimately the electric and magnetic fields are continuous over grating discontinuities, not the envelopes functions. However, for the weak gratings we are considering here, Maxwell's *saltus* conditions reduce to the continuity of the $\mathcal{F}_\pm$ to a good approximation.

B. Stability

For the stationary solutions given by Eqs. (19)–(21) to be experimentally observable, they must be stable. When we have a pair of solutions x_l, x_r and $-x_l, -x_r$ then one, two, or none of the solutions might be stable. Since these solutions peak in different gratings, they have different energies (Q) and one might expect that the solution with the lower energy to be stable.

The usual exact way to determine stability is to perform a linear stability analysis of the solutions or to simulate the solutions with a full time dependence on a computer. However, in Newtonian dynamics the stability of a stationary particle is determined by whether or not it is at a local minimum of the potential. Hence if we could define a potential for our solutions, then determining stability would be a simpler task. Using the EPP approach this method is possible.

As an example we consider the case where the only grating parameter to change across the interface is κ. This case is of particular interest as such step gratings have reduced thresholds for the launching of gap solitons [8]. The perturbation matrix in Eqs. (1) and (2) is then

$$V_{11} = V_{22} = 0, \tag{27}$$

$$V_{12} = V_{21} = \begin{cases} (\kappa_r - \kappa_l)\mathcal{H}(x), & \bar{x} < 0 \\ (\kappa_l - \kappa_r)\left[1 - \mathcal{H}(x)\right], & \bar{x} > 0, \end{cases} \tag{28}$$

where κ_l, κ_r are the grating strengths on the left- and the right-hand side, respectively, and $\mathcal{H}(x)$ is the Heaviside

Lorentz step function. This perturbation is then used in the EPP Eqs. (16)–(18). The resulting equations are

$$\frac{d\bar{x}}{dt} = v, \tag{29}$$

$$\mathcal{P} = \frac{2\kappa v\gamma}{\Gamma_x}\alpha^2 \sin\delta + \frac{4\kappa\Gamma_s v\gamma^3}{\Gamma_x^2}\alpha^4(\sin\delta - \delta\cos\delta), \tag{30}$$

$$\frac{d\mathcal{P}}{dt} = F, \tag{31}$$

where, for $\bar{x} < 0$, the force F is defined as

$$F = \frac{\alpha^2(\kappa_l - \kappa_r)}{2\Gamma_x}\sin^2(\delta_l)\frac{\cosh^2\theta\cos\delta_l + \sin^2\delta_l/2}{\left(\cosh^2\theta - \sin^2\delta_l/2\right)^2}, \tag{32}$$

$$\theta = \kappa_l \sin\delta_l \bar{x}. \tag{33}$$

For $\bar{x} > 0$ the force is similar to Eq. (32), but with $\delta_l \mapsto \delta_r$ and $\theta = \kappa_r \sin\delta_r \bar{x}$. Note that from Eqs. (31) and (32) $d\mathcal{P}/dt = 0$ only if $\delta > \pi/2$ or if $\kappa_r = \kappa_l$. When $\kappa_r = \kappa_l$, then $F \equiv 0$ and stationary solitons can exist everywhere, as expected for a uniform grating. If $\kappa_r \neq \kappa_l$, then according to the EPP approach stationary solutions can exist only if $\delta > \pi/2$ and when

$$\theta = \pm\cosh^{-1}\sqrt{\frac{-\sin^2(\delta/2)}{\cos\delta}}, \tag{34}$$

as otherwise there would be a force on the soliton. This agrees with our result in Sec. III A that stationary solitons only exist when $\delta > \pi/2$. In the low velocity limit the momentum [given by Eq. (30)] is proportional to the soliton's velocity and the left-hand side of Eq. (32) is independent of velocity. In this case we can define a potential as

$$V(x) = -\int_{-\infty}^{x} F(x')dx'. \tag{35}$$

For stationary gap solitons this is a true potential, while for slowly moving solitons the potential is an approximation. This potential can be used in determining the stability of stationary soliton solutions. Figure 3 shows a typical potential with $\kappa_l = 1\,\mathrm{cm}^{-1}$ and $\kappa_r = 1.1\,\mathrm{cm}^{-1}$, which has a local minimum in the left-hand medium and a local maximum in the right-hand medium. Hence the EPP predicts that the stationary solution peaked in the left-hand medium are stable and the one peaked in the right-hand medium is unstable. This agrees with our numerical studies. Note that the stable soliton in the left-hand medium has the lower energy, as suggested at the start of the section.

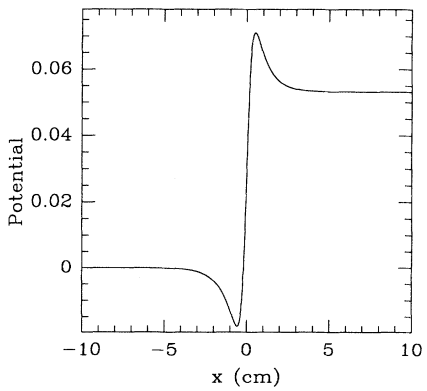

FIG. 3. Plot of the EPP potential corresponding to the case where the grating strength κ increases discontinuously at the origin. This potential implies that stationary solutions peaked in the left-hand medium are stable while those in the right are unstable. Here $\kappa_l = 1\ \mathrm{cm}^{-1}$ and $\kappa_r = 1.1\ \mathrm{cm}^{-1}$ with the interface at $x = 0$.

The exact form of the potential defined by Eq. (35) is valid only for perturbations where the strength of κ changes discontinuously across the interface. More general perturbations would include changes in the nonlinearity and the phase of the second grating. In this general case the perturbation matrix V takes the form (for $x < 0$)

$$V_{11} = \left[(\Gamma_{xr} - \Gamma_{xl})\,|\mathcal{F}_-|^2 + (\Gamma_{sr} - \Gamma_{sl})\,|\mathcal{F}_+|^2\right]\mathcal{H}(x), \tag{36}$$

$$V_{12} = V_{21}^* = (\kappa_r - \kappa_l e^{i\phi})\mathcal{H}(x), \tag{37}$$

$$V_{22} = \left[(\Gamma_{xr} - \Gamma_{xl})\,|\mathcal{F}_+|^2 + (\Gamma_{sr} - \Gamma_{sl})\,|\mathcal{F}_-|^2\right]\mathcal{H}(x). \tag{38}$$

The analysis for the more general perturbation follows exactly the method presented above. As Eqs. (15)–(18) are linear in V, each term in the perturbation matrix can be treated separately, with the final force being the sum of all the individual forces. In all cases a potential defined by Eq. (35) can be used to determine the stability of the stationary gap solitons. Since the potential depends on χ^2 it is correctly defined only for a stationary gap soliton and is an approximation for slowly moving solitons. However, these potentials arising from the EPP approach allow us to make accurate predictions about the stability of the stationary gap solitons in regimes where no analytic results are known.

IV. MOVING SOLITONS AND STATIONARY INTERFACES

In Sec. III the EPP approach was used to predict the stability of stationary solutions at an interface. However, once the gap soliton has a nonzero velocity the EPP equations cannot be solved exactly. Instead we solve the EPP equations numerically, which is faster than resorting to full numerical simulations. As in Sec. III, we consider an interface between two different uniform gratings. However, as the soliton is moving there is a difference between the coupled mode equations and the MTM and the two cases have to be treated separately.

We consider only the case of a discontinuous change in κ. The perturbation matrix is again given by Eqs. (27) and (28). The resulting EPP equations are thus the same as in Sec. III B. In contrast to the preceding section, we now consider a soliton located at $|\bar{x}| \gg 0$ moving with a velocity v. While the gap soliton does not cross the interface, the EPP force on the gap soliton changes continuously. If the soliton is in the left-hand medium, then the right-hand medium is treated as a perturbation;

however, when the gap soliton crosses the interface the roles are reversed. This abrupt change is reflected in the EPP force being discontinuous at the origin and is an artifact of the EPP method. We assume that as we have a soliton, then at the interface there is no significant loss of energy due to radiation and that we always have only a single pulse in the system. Our numerical simulations support this assumption, except in extreme cases where the gap soliton is found to break up.

Recall that gap solitons are defined by two parameters δ and χ. Thus for each different interface we need to test the EPP approach over a wide range of parameters. We have divided the (δ, χ) plane into four main regions, as shown in Fig. 4. Regions 1 and 4 are discussed briefly, while we examine regions 2 and 3 in more detail. In region 4, solitons are small, wide, and slowly moving. In this region both the MTM and the NLCME reduce to the nonlinear Schrödinger equation. As Aceves *et al.* [9] have successfully applied the EPP approach to the NLSE, we do not discuss this region in detail. In this region the potential defined by Eq. (35) can be used to determine accurately the dynamics of the gap soliton's motion as in this limit the EPP approach reduces to that of a particle moving in a potential well.

Figure 5 compares the results from the EPP approach to the exact numerical simulations for the NLCME in region 3 of Fig. 4. In this region the gap soliton is slow and strongly peaked. The dashed line shows the EPP trajectories through (x, χ) space, while the solid line shows the exact trajectories. In these simulations the gap soliton parameter $\delta = 2$, while the initial velocity is in the range $-0.5v_g < v < 0.5v_g$. Further $\kappa_l = 1$ cm^{-1} and $\kappa_r = 1.1$ cm^{-1}, while the other parameters remain constant across the interface. The potential corresponding to this perturbation is shown Fig. 3. The EPP force, given by Eq. (32), is velocity dependent as both α and θ depend on v and so the motion of the gap soliton cannot be reduced to that a particle moving in a potential well. As the force depends only on the square of the velocity, in the low velocity regime we can assume a velocity independent force and hence we can define an approximate potential. It should be noted that the general features of the potential agree with the general features of the phase plots. According

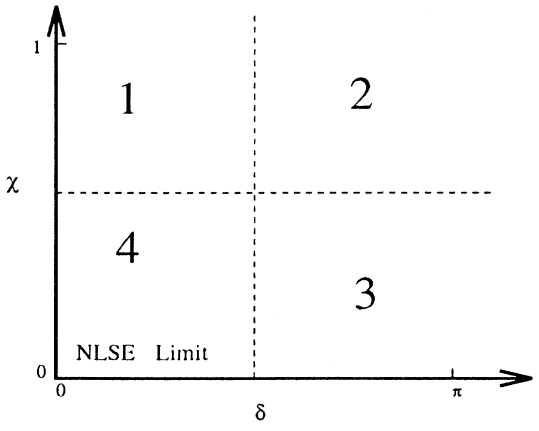

FIG. 4. Different regions of the (δ, χ) plane.

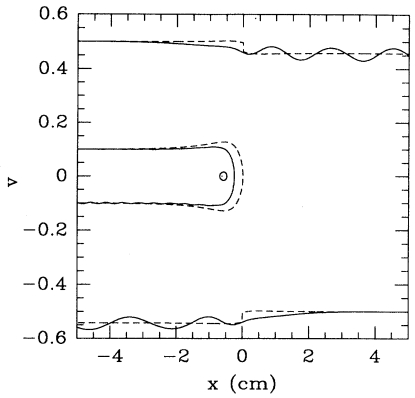

FIG. 5. Various trajectories in the (v, x) plane. The dotted lines shows the results from the EPP approach, the solid lines the results from the exact numerical simulations. The potential in this case is given in Fig. 3

to the potential, the high κ region has a higher potential than the left-hand side. Thus we would expect that low velocity gap solitons in the left-hand medium are reflected by the interface, while those that penetrate have a reduced velocity, as is the case in Fig. 5. In contrast, gap solitons moving from right to left speed up as they cross the interface. A main feature of the phase plots in this region is the oscillations of the gap soliton after it has interacted with the interface. In most cases these oscillations eventually decay for both the MTM and the NLCME solitons. In more severe cases the oscillations can cause the NLCME soliton to split into two solitons moving with a different velocity. The EPP approach, as presented here, is unable to capture this feature as in the EPP approach the gap soliton is not allowed any internal degrees of freedom corresponding to oscillations. However, the EPP approach does correctly predict the average velocity after the interaction.

In region 2 the solitons are fast and narrow. Here the difference between the MTM soliton and NLCME soliton is the greatest. As the MTM soliton is a true soliton, the effect of the interface is not as severe as in the case of the gap soliton, which is a solitary wave. Figure 6 shows a phase plot for a gap soliton with $\delta = 2.3$ and $\chi = 0.7$ for both the EPP (dotted line) and the full simulations. As in the previous plots, $\kappa_l = 1$ cm^{-1} and $\kappa_r = 1.1$ cm^{-1}. The velocity of the gap-soliton oscillates about the EPP velocity with the amplitude of the oscillations decaying as the soliton moves away from the interface (at $x = 0$).

When the change in grating strengths at the interface becomes larger our EPP model breaks down. The reason for this is shown in Fig. 7, where the left-hand plot shows the initial soliton and the right-hand plot shows the field distribution after interacting with the interface. In this case $\kappa_l = 1$ cm^{-1} and $\kappa_r = 2$ cm^{-1}, while $\delta = 2.3$ and $\chi = 0.7$. Since the EPP approach assumes that we only have small perturbations, it is not unexpected that it will fail for large perturbations. Clearly in this regime our assumption that the field remains as a single soliton is incorrect. To accurately model this region with an EPP approach we would have to include both a reflected and

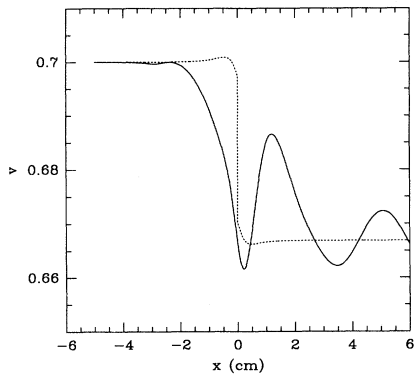

FIG. 6. Trajectory in the (v, x) plane. The dotted line shows the results from the EPP approach, the solid lines the result from the exact numerical simulation. The parameters for the grating are the same as in Fig. 3.

a transmitted pulse, which would double the complexity of the system.

In region 2 the EPP approach is more accurate for the massive Thirring model, presumably as the MTM is exactly integrable. Thus the MTM soliton is more robust and less likely to break up.

In region 1 of Fig. 4 the solitons are fast and wide and the central frequency is close to the upper band edge. Due to the velocity dependence of the EPP force, we are unable to define a potential in this region though the EPP approach is still accurate. In order to obtain the EPP results we need to integrate the EPP equations numerically. As the EPP equations are coupled ordinary differential equations, this is of course much faster than solving the full partial differential equations. The general features of trajectories in this region is that a gap soliton's velocity increases if it moves into a region where κ is lower and the velocity decreases when it moves into a region of high κ. These general features are in qualitative agreement with the low velocity potential, where the region of lowest κ is also the region where the potential is the lesser. Since the main features are similar to the other regions where the EPP holds we present no figures for region 1.

V. DISCUSSION

In this paper we concentrated on discontinuities of κ. One reason for this is that we have proposed a scheme for launching gap solitons that rely on such perturbations and thus it is important to know how these perturbations affect the gap soliton's motion. In contrast, the strength of the nonlinearity is an intrinsic material property and thus in order to change the strength of the nonlinearity the grating would have to overlap two different materials. Such structures are more difficult to achieve in the context of optical fiber Bragg gratings and thus we have not examined them in much detail. However, the EPP approach presented here can be applied to such cases.

In the case of more complicated perturbations, the perturbations can be broken down into simple perturbations, each of which can be treated separately via the EPP approach. For each perturbation the EPP "force" can be derived and the total force is the sum of all the forces. Thus our approach of only treating perturbations to κ is justified in the case of a more general perturbation, as the contribution to the force from a perturbation to κ is given by our approach irrespective of any other perturbations.

The EPP approach presented here involves a perturbation matrix V. However, for a nonlinear perturbation V is not uniquely defined. Consider a term proportional to $\mathcal{F}_-\mathcal{F}_-^*\mathcal{F}_+$, which could arise from a perturbation in the nonlinearity; then this term can be included in either the V_{11} or the V_{12} element in Eq. (1). However, in the cases we have considered this ambiguity does not affect the final results. If the perturbation can be expressed in such a way as to ensure that V is Hermitian, then this form is usually preferable as, for a Hermitian matrix, the EPP equations can be written in a simpler form.

VI. CONCLUSION

In this paper we have presented a general framework for treating perturbations to gap solitons, by using an effective particle picture. Although the EPP is very general, in the examples we have concentrated on abrupt perturbations to the strength of the grating. We have

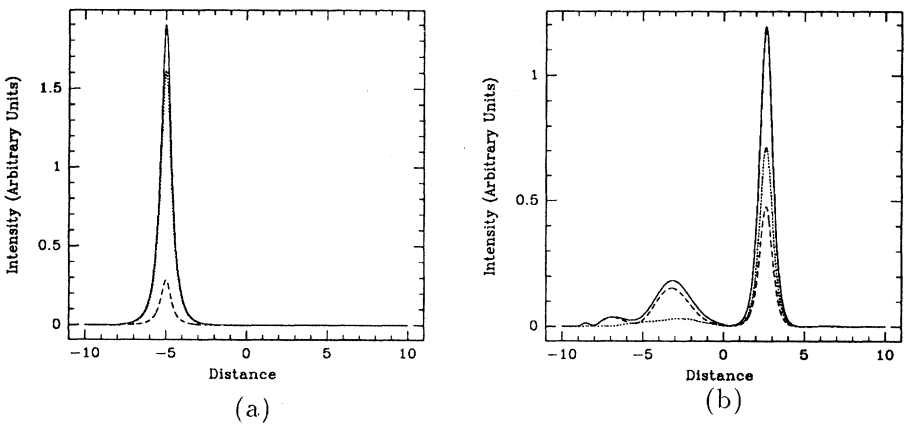

FIG. 7. (a) Initial profile of a gap-soliton with $\delta = 2.3$ and $\chi = 0.7$. (b) Electric field profile after interaction with the interface. The solid line shows the total intensity, the dotted line represents $|\mathcal{F}_+|^2$, and the dashed line $|\mathcal{F}_-|^2$. The interface is at $x = 0$ with $\kappa_l = 1$ cm^{-1} and $\kappa_r = 2$ cm^{-1}.

also examined the effect of perturbations to the MTM model to provide a comparison for the result of the NLCMEs.

The EPP approach is successful over a wide range of initial conditions, but our current approach fails for the NLCME in extreme cases where the gap soliton breaks up. The results for the MTM in this limit are more accurate as the MTM soliton is more robust. The reason for this is that in extreme cases the NLCME soliton is more likely to break up at the interface than the MTM soliton. As our model assumes that we always have only one gap soliton, it is unable to treat this case. However, the model should be capable of being easily extendable to dealing with multisolitons, and this is not a fundamental flaw of the EPP approach.

ACKNOWLEDGMENTS

This work was supported in part by the Australian Photonics CRC and by the Australian Research Council. The Optical Fibre Technology Centre is a member in the Australian Photonics CRC. N.G.R.B. is grateful for the APA support.

[1] H. G. Winful, J. H. Marburger, and E. Garmire, Appl. Phys. Lett. **35**, 379 (1979).
[2] W. Chen and D. L. Mills, Phys. Rev. B **36**, 6269 (1987).
[3] W. Chen and D. L. Mills, Phys. Rev. Lett. **58**, 160 (1987).
[4] A. B. Aceves and S. Wabnitz, Phys. Lett. A **141**, 37 (1989).
[5] N. D. Sankey, D. F. Prelewitz, and T. F. Brown, Appl. Phys. Lett. **60**, 1427 (1992).
[6] R. W. Boyd, *Nonlinear Optics* (Academic, San Diego, 1992).
[7] C. M. de Sterke and J. E. Sipe, Opt. Lett. **18**, 269 (1993).
[8] N. G. R. Broderick, C. M. d. Sterke, and J. E. Sipe, Opt. Commun. **113**, 118 (1994).
[9] A. B. Aceves, J. V. Moloney, and A. C. Newell, Phys. Rev. A **39**, 1809 (1989).
[10] C. M. de Sterke and J. E. Sipe, in *Progress in Optics*, edited by E. Wolf (North-Holland, Amsterdam, 1994), Vol. XXXIII, Chap. III, pp. 203–260.
[11] C. M. de Sterke and J. E. Sipe, Phys. Rev. A **42**, 550 (1990).
[12] D. J. Kaup and A. C. Newell, Lett. Nuovo Cimento **20**, 325 (1977).
[13] E. A. Kuznetsov and A. V. Mikhailov, Theor. Math. Phys. **30**, 193 (1977).
[14] C. M. de Sterke and J. E. Sipe, Phys. Rev. A **43**, 2467 (1991).
[15] M. J. Steel and C. M. de Sterke, Phys. Rev. A **48**, 1625 (1993).